THE JOURNAL OF PHYSICAL CHEMISTRY B

Article

pubs.acs.org/JPCB

# Imaging and Measuring Single-Molecule Interaction between a Carbohydrate-Binding Module and Natural Plant Cell Wall Cellulose

Mengmeng Zhang,[†] Sheng-Cheng Wu,[‡] Wen Zhou,[§] and Bingqian Xu[†,*]

[†]Single Molecule Study Laboratory, Faculty of Engineering and Nanoscale Science and Engineering Center, University of Georgia, Athens, Georgia 30602, United States

[‡]Complex Carbohydrate Research Center and Department of Cellular Biology, University of Georgia, Athens, Georgia 30602, United States

[§]Department of Chemical Engineering, Michigan Tech University, Houghton, Michigan 49931, United States

Supporting Information

**ABSTRACT:** The affinitive interaction between a carbohydrate-binding module (CBM3a) and natural crystalline cellulose was visualized and measured at the single-molecule level. Noncontact high resolution imaging by atomic force microscopy (AFM) was used to follow the binding process, in real time, of CBM3a-functionalized 6 nm gold nanoparticles (GNPs) to the cell wall polymers on poplar stem sections. The GNP−CBM3a complexes were found to bind to the cellulose surface, closely aligning along the cellulose fibril axis. The binding details were further confirmed and studied by single-molecule recognition imaging and AFM single-molecule dynamic force spectroscopy (SMDFS) using a CBM3a-functionalized AFM tip. The unbinding force was measured to be 44.96 ± 18.80 pN under a loading rate of 67.2 nN/s. This research provides a radical method for the study of single-molecule affinity between CBM and cellulose that is critical to the engineering of novel cellulolytic enzymes.

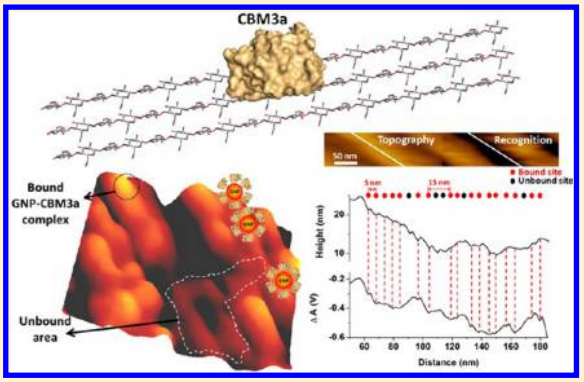


## INTRODUCTION

Enzymatic hydrolysis of renewable lignocellulosic biomass (primarily plant cell walls) is critical for biofuel production and has been evolved into a major focus of study over the years.[1,2] As the skeleton of plant cell walls, cellulose is the major polysaccharide rich in organic carbon which comprises a linear chain of $\beta$ (1→4) linked D-glucose units. The natural degradation of plant cell walls involves molecular interactions between microbial cellulolytic enzymes and well-assembled polysaccharides such as interwoven cellulose microfibrils trapped in disordered polymer matrix (e.g., xylans, pectins, and lignin).[3,4] The complex structure of the plant cell walls, especially the cross-linking between the polysaccharides and lignin, created a huge barrier, or biomass recalcitrance, in cellulose degradation.[5,6] The cross-linked protective polymeric substances are traditionally removed by caustic chemical treatments to make the cellulose fully exposed for enzymatic hydrolysis.[7] Comparatively, direct enzymatic hydrolysis of cellulose has proven to be more promising and environment-friendly.[8,9] However, it has been a great challenge to improve the efficacy of enzymatic hydrolysis, as little is known microcosmically about the real structure of plant cell walls and the enzymes' access to and interaction with the embedded polysaccharides.[10,11] Therefore, a more profound understanding of substrate-enzyme interactive mechanisms down to single-molecule level is crucial to the enzymatic convertion of the biomass into fermentable sugars, thus ultimately optimizing production of bioethanol.[12]

Cellulolytic enzymes are generally modular proteins with independent catalytic domains and noncatalytic carbohydrate-binding modules (CBMs). As the first and key step in the hydrolysis process, the interactions between the plant cell wall carbohydrates and a group of unit contiguous amino acid sequences (i.e., CBMs) in cellulolytic enzymes need to be quantified.[13] The main function of CBMs is to recognize the target carbohydrate substrate and then convey their catalytic counterparts to the substrate surface for effective hydrolysis at intimate proximity.[2] More than 60 sequence-based families of CBMs have been identified and classified in the carbohydrate-active enzymes (CAZy) database.[14] On the basis of experimentally verified structural and functional similarities, cellulose-specific CBMs are classified into three types, binding to specific surfaces of insoluble crystalline cellulose (type A), individual $\beta$ (1→4) glucan chains (type B) and small sugars (type C).[13] One of the type A CBMs, CBM3a, is a family 3 carbohydrate-binding module from the cellulosomal scaffoldin subunit *CipA* of *Clostridium thermocellum*. It has been both theoretically and experimentally proven to bind specifically to

**Received:** May 14, 2012
**Revised:** July 27, 2012
**Published:** July 31, 2012

   dx.doi.org/10.1021/jp304686q | *J. Phys. Chem. B* 2012, 116, 9949−9956

crystalline cellulose.[15,16] Different from hemicelluloses and amorphous cellulose, which are readily digestible, the crystalline region of cellulose microfibrils is highly resistant to hydrolysis due to its rigid structure.[17] A detailed knowledge on the structure and function of CBMs, especially their actions on carbohydrate substrates at single-molecule level will definitely offer a new insight into the mechanisms of carbohydrate-enzyme recognition and interaction.

High resolution electron microscopy (EM) imaging techniques, such as scanning electron microscopy (SEM)[18,19] and transmission electron microcopy (TEM),[20] are widely used to observe the plant well wall structure and carbohydrate-enzyme interactions. By labeling pretreated plant cell wall cellulose with fluorescent tags, such as semiconductor quantum dots (QDs)[21] and fluorescent proteins (FPs),[22,23] specific binding sites and unique CBM behaviors have been observed. Nevertheless, the pretreatment procedures used for the plant materials are time-consuming and most likely have altered the native structure or organization of the plant cell walls. In addition, neither SEM nor TEM provides detailed 3D information on the roughness and height of plant cell wall surfaces. Comparatively, high resolution atomic force microscopy (AFM) experiments,[24,25] if properly and carefully designed, offer a distinctive 'biophysical' methodology to directly visualize plant cell wall surface and pretreated cellulose microfibrils at nanoscale resolution and with the least perturbation of sample *in situ*.[26,27] More importantly, the binding affinity between a CBM and its substrate can be measured with pico-Newton sensitivity.[25,28]

Recently, several remarkable progresses have been made in cellulose-CBM interaction study using AFM. One is *in situ* AFM observation of *Tr*Cel7A molecules (a whole cellobiohydrolase from *Trichoderma reesei)* with both cellulose-binding and catalytic modules) sliding on single crystalline cellulose, which showed that the cellulose-binding domain (CBD) had no active roles in cellulose hydrolysis except to increase the enzyme concentration on the substrate.[29] Another study of real-time AFM observation and measurement proved the morphological changes in cellulose single crystals during the hydrolysis by cellobiohydrolase I (CBH I) from *T. reesei*.[30] Some other imaging works are performed on dried plant cell wall−CBM/enzyme complexes,[28] the information about how and how strong the CBMs interact at real time with natural plant cell wall cellulose in an aqueous condition is still missing. Although the unique architecture of active CBM binding sites and their binding affinity on the crystalline cellulose surface have been widely studied by molecular modeling,[31,32] the absence of experimental data on the cellulose−CBM binding affinity on an intact plant cell wall surface makes it difficult to evaluate the theoretical molecular modeling results. Eventually, the lack of consensus between the theoretical prediction and experiment support will hinder the design and modification of effective cellulolytic enzymes, accordingly obstructs biofuel production.[10]

In this work, we monitored the binding activity of CBM3a to the poplar cell wall cellulose in real time using CBM3a-functionalized gold nanoparticles (GNPs). We followed it up by single-molecule recognition imaging directly using the CBM3a-functionalized AFM tip to map out the binding events across the plant cell wall surface samples.[33] All the experiments were performed on untreated microtomed poplar stem sections. To quantify the binding affinity, we also measured the interaction forces between the cellulose and CBM3a using AFM single-molecule dynamic force spectroscopy (SMDFS). The results of this study offer a direct, real-time and quantitative observation of the binding activities between CBM3a and plant cell wall cellulose at the single-molecule level.

## MATERIALS AND METHODS

**Preparation of Recombinant CBM3a (Supporting Information, SI-I).** The sequence encoding CBM3a was amplified by PCR from the genomic DNA of *C. thermocellum* strain ATCC 27405 and cloned into an expression vector, pET28b. The resulting plasmid, pCBM3a, was transformed into *Escherichia coli* host strain Tuner(DE3) for protein induction. The $(His)_6$-tagged CBM3a was purified by immobilized metal affinity chromatography (IMAC) essentially as described by Blake et al.[16]

**Poplar Sample Preparations for GNP−CBM3a Binding Observation and Recognition Imaging.** Fresh stems of poplar plant (*Populus alba*) was obtained from the University of Georgia campus greenhouse. Stem sections of 50 $\mu$m thick were cut by microtome in the Electron Microscopy Lab (Department of Plant Biology, University of Georgia). The poplar sections were placed between two clean glass slides at ambient temperature to prevent distortion.[27] Before scanning, the sample was immobilized on a glass slide with a minute amount of epoxy glue and air-dried. The sample was fixed onto an AFM flow cell,[34] which was then filled with 0.3 mL of Binding Buffer (10 mM Tris-Cl, pH 7.5, and 150 mM NaCl) for GNP−CBM3a binding observation and recognition imaging.

**Gold Nanoparticle Functionalization.** The gold nanoparticles (GNPs; 6 nm, 1 mL from Nanopartz Inc.) was incubated with the DTSP−ANTA (shown as NTA for short hereafter) cross-linker (2 mg/mL, 0.25 mL). The synthesis procedure of NTA cross-linker is included in Supporting Information, SI-II. After 2−3 h, the mixture was reacted with $NiCl_2$ solution (50 mM, 15 $\mu$L) for 30 min. The modified GNPs suspension was centrifuged for 15 min at 13,000 g in a SORVALL BioFuge Pico Microcentrifuge and then washed 3 times with the binding buffer. Finally, the pelleted GNPs were incubated in CBM3a-$(His)_6$ solution (20 $\mu$g/mL, 10 $\mu$L) with addition of 1 mL of binding buffer. Before use, the GNP−CBM3a complexes were centrifuged again to remove excessive CBM3a and the pellet was redispersed in 1 mL of binding buffer for future imaging. The UV−vis absorbance measurements were carried out on a UV-1700 spectrophotometer at room temperature (Shimadzu Scientific Instruments).

**AFM Experimental Settings.** The PicoPlus Molecular Imaging system together with a PicoScan 3000 Controller was used in this work. An Agilent multipurpose AFM scanner was used for scanning within an area size of 10 $\mu m^2$. All the images were taken using Top magnetic AC (TopMAC) mode under PicoTREC (Agilent Technologies, Santa Clara, CA) with CS-10 silicon AFM tips (Nanoscience Instruments, nominal spring constant $\approx$ 0.1 N/m). The whole system was enclosed by a PicoPlus Isolation Chamber to be shielded from environmental interference.

**AFM in Situ Imaging Operation for GNP−CBM3a Binding Observation.** After several high resolution images were obtained on a small area of the microtomed poplar stem surface, the scanning was stopped and 0.2 mL of GNP−CBM3a suspension was gently injected into the flow cell. The scanning was then restarted to monitor the whole binding process in the following 7 h.


dx.doi.org/10.1021/jp304686q | J. Phys. Chem. B 2012, 116, 9949−9956

## RESULTS AND DISCUSSION

The surface of natural plant stem section is rough and the components embedded in the cell walls are extremely complicated, making it difficult to directly observe the binding of CBM3a (with the 3D dimension of 3 nm × 3 nm × 4.5 nm)[15] to crystalline cellulose surface. Therefore, to follow the binding events of CBM3a to plant cell wall cellulose, we choose to monitor the 6 nm CBM3a-coated GNP complexes anchoring on the sample by high-resolution in situ imaging in real time. To coat the GNPs with CBM3a, we started with the synthesis of a NTA cross-linker (Supporting Information, SI-II). Then GNPs were chemically functionalized with the cross-linker via the S−Au bonding.[35] Finally, the recombinant CBM3a-$(His)_6$ molecules were attached onto the cross-linker-modified GNP surface (Figure 1a and Materials and Methods).

As shown in Figure 1b, the color of the pure 6 nm GNPs suspension is dark red (left panel) and gradually changes into light purplish after NTA-cross-linker and CBM3a functionalization (right panel). The color changes suggest the shift of the surface plasmon resonance (SPR) peaks of the GNPs at each surface reaction stage, but only this information cannot give the whole morphological condition of the modified GNPs. Therefore, to make sure that our modification was successful without any severe aggregation, we used the UV−vis spectrophotometer to quantify the SPR peak shifts. We measured the UV−vis absorbance properties of the GNPs after each reaction step using a UV−vis spectrophotometer. As shown in Figure 1c, the characteristic absorption peak of pure 6 nm GNP appears at 516 nm before functionalization (black curve). After the addition of NTA cross-linker and $Ni^{2+}$ solution, the absorption peak shifts to 518 nm (red curve), showing an increase of the diameter of GNPs due to the formation of Ni−NTA monolayer on the surface of GNPs via Au−S bonding. When CBM3a-$(His)_6$ was mixed with the GNP-cross-linker complexes, the absorption peak became slightly wider and shifted to 523 nm (blue curve), indicating a further coverage of the cellulose-binding module chelating the Ni-NTA monolayer. Though several factors can cause the shift of SPR peaks (e.g., size, shape and local environment),[36] it is obvious in this case that the spontaneous S−Au and Ni−histidine tag interactions primarily causes the changes in particle size and hence the color. Therefore, the UV−vis absorption spectrum measurements demonstrated the morphological alterations of the GNPs before and after modification due to the linkage of of CBM3a-$(His)_6$ on the GNP surface, demonstrating the success of the modifications.

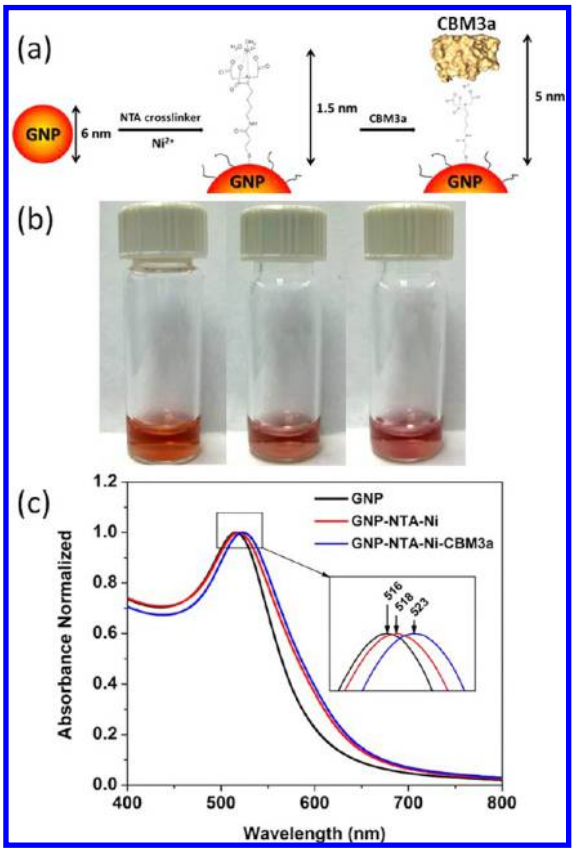


**Figure 1.** Schematics of GNP functionalization and characterization by UV−vis spectrophotometer. (a) Brief synthesis procedure of the gold nanoparticle (GNP)−CBM3a complex. The GNP, Ni−NTA cross-linker, and CBM3a molecule (Protein Data Bank, PDB code: 1NBC, The CBM3a model is generated by molecular visualization software PyMOL (version 0.99rc6).) and is not drawn to scale. (b) Color changes of pure GNPs to the CBM3a-functionalized GNPs. (c) Characteristic UV−vis absorbance peaks of 6 nm GNPs at 516 nm, Ni−NTA-cross-linker bound GNPs at 518 nm and CBM3a-linked GNP complexes at 523 nm (inset: highlight of the peak shifts). The peak shifts indicate the morphological changes of the GNPs after each reaction step.

To observe the binding process of the GNP−CBM3a complexes to the cellulose, we first used a bare AFM tip to find a target area on the poplar sample surface with representative features (i.e., clear crystalline cellulose microfibrils in a parallel arrangement) and then stopped scanning. After the injection of GNP−CBM3a suspension into the flow cell,[34] the scanning was restarted and the whole binding process was continuously monitored and recorded for 7 h in the same selected scanning area. Figure 2 shows the snapshots of 4 AFM topographic and amplitude images of the GNP−CBM3a complexes binding on the sample surface at time 0 min (Figure 2a and 2e), 70 min (Figure 2b and 2f), 327 min (Figure 2c and 2g), and 395 min (Figure 2d and 2h). At the very beginning, the parallel cellulose microfibrils with each at a diameter of 10−20 nm were clearly observed on the sample surface. A few irregular dots in various sizes embedded among the microfibrils are most likely other natural polymers or membrane debris in the plant cell walls.[26] With the GNP−CBM3a complexes gradually bound to the cellulose, more and more round spots in diameter of 30−40 nm appeared on the cellulose surface. Beginning at ∼70 min the GNP−CBM3a complexes were found to align with each other to form a parallel structure and finally cover about 80% area of the sample surface at ∼400 min. After about 395 min, the morphology of the sample surface no longer showed much difference, suggesting that the binding of the GNP−CBM3a complexes onto the cellulose was saturated. The selected area in the red square shows clearly how the morphology changes during the whole binding process. The actual size of a single GNP−CBM3a complex is supposed to be around 16 nm in diameter (estimated as shown in Figure 1a), while the apparent size shown in the AFM images is 30−40 nm (Figure 2c and Figure S1, Supporting Information) due to the AFM tip broadening effect and compression of molecules caused by the force applied.[37]

In a previous study, (CdSe)ZnS quantum dots (QDs) directed by CBM3a were used to achieve direct labeling of the planar face on an isolated single crystalline cellulose.[21] Electron microscopy results showed that these QDs directed by CBM3a


dx.doi.org/10.1021/jp304686q | J. Phys. Chem. B 2012, 116, 9949−9956

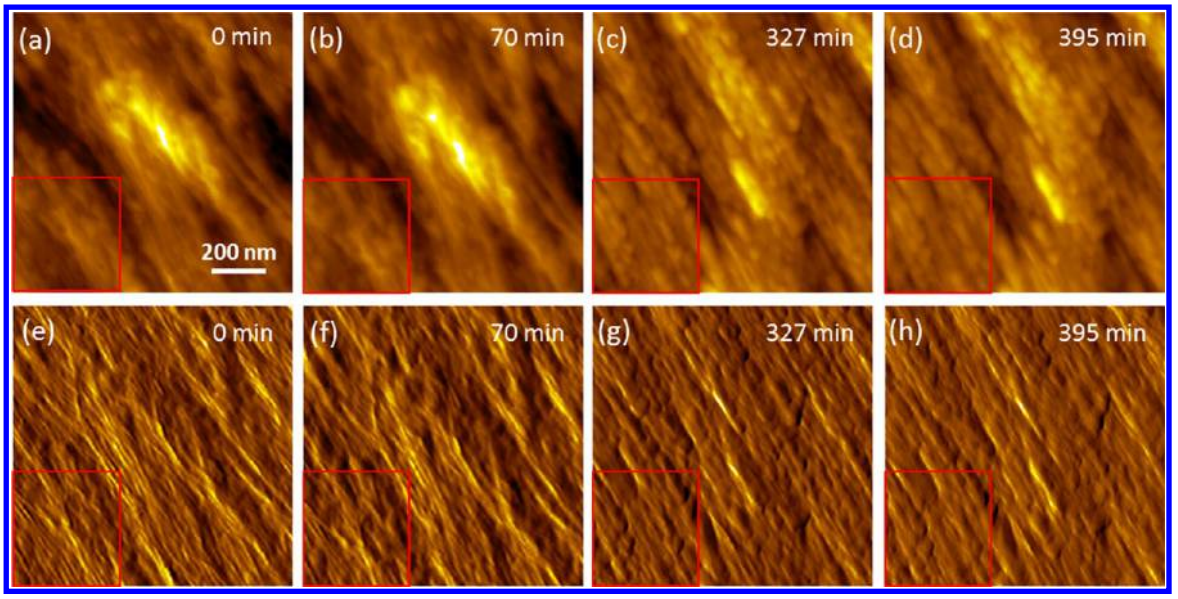


**Figure 2.** In situ real-time imaging of AFM topographic and amplitude images of the GNP−CBM3a complexes binding on the poplar cell wall surface: (a−d) topographic image; (e−h) amplitude image; (a and e) 0 min; (b and f) 70 min; (c and g) 327 min; (d and h) 395 min. In the beginning, the cellulose microfibrils in the diameter of 10−20 nm are clearly observed on the sample surface in a well-paralleled arrangement. Gradually, spots in diameter of 30−40 nm increasingly appear on the cellulose surface and eventually cover about 70% area of the control sample surface. The area in the red square highlights the morphology alteration during the imaging time period.

probes aligned precisely in a linear sequence along the hydrophobic (110) planar face of cellulose. In our observation on natural plant cell walls, the GNP-guided CBM3a still bind to the area of crystalline cellulose microfibrils in a linear arrangement along the microfibril axis, although the specific planar face of crystalline cellulose was not seen clearly in the images due to the complexity of the natural plant cell walls structure. Nevertheless, our results directly demonstrate that CBM3a is able to bind to and densely align along the natural, parallel crystalline cellulose surprisingly quickly (within 7 h). In the control experiments on crystalline cellulose with pure GNPs (Supporting Information SI−III, a) and amorphous cellulose with GNP−CBM3a complexes (Supporting Information, SI−III, b), no obvious specific binding was observed under these experimental conditions. To unambiguously prove that GNP−CBM3a chemically binds to crystalline cellulose, further experiments on the binding specificity and binding affinity were carried out.

To reveal the binding details, we selected one of the images at 395 and 0 min of the same area for comparison. Figure 3 depicts the representative area generated from the red square in Figure 2, exhibiting the detailed changes of morphology. Figure 3b is the height analysis generated from the blue lines showing the morphological changes before (Figure 3a) and after binding (Figure 3b). Before the GNP−CBM3a binding, the image shows most of the clear crystalline cellulose microfibril structure (Figure 3a) with a diameter of 10−20 nm (Figure 3c). With the binding of GNP−CBM3a, crystalline cellulose microfibril structure gradually disappeared and the topography showed close alignment of GNP−CBM3a (Figure 3b) with a larger size of 30−40 nm (Figure 3c). A representative alignment of the particles is marked in the red square and highlighted in the 3D figure as shown in Figure 3d. The locations of the GNP−CBM3a complexes on the cellulose surface were partially highlighted at the top by dashed, black circles. The inset of Figure 3d shows the cross-section generated from the two adjacent complexes labeled by double-headed arrow representing the distance, $D$, between the centers of the two complexes. $D$ was measured to be around 50 nm and the separation space between the opposite edges of two bound complexes is about 20−30 nm. This separation measured is larger than the reported average separation distances between two quantum dotes binding to individual CBM3a molecules that already bond on (110) face of a single crystalline cellulose.[21] One possible reason is that the GNP−CBM3a complexes are larger in size than the single CBM3a molecules, thus separating apart at a larger space when binding along the crystalline cellulose microfibrils due to steric hindrance during targeting. In addition, some areas on the sample surface is inevitably covered by other noncellulose carbohydrate polymers (invisible here) due to the impurity of the natural plant cell walls, making it impossible for the CBMs to bind to and thereby enlarging the space between the bound complexes. One example of the cellulose surface exposed to the buffer solution without any CBM3a binding is shown in Figure 3d (circled by the white dashed line). The single alignment strip of GNP−CBM3a complexes on the inferred hydrophobic (110) cellulose surface is marked by a black, dashed rectangle and highlighted on the schematic drawing in Figure 3e, illustrating the distribution of GNP−CBM3a complexes on a single crystalline cellulose.

Next, we studied the direct binding of CBM3a to crystalline cellulose on natural plant dell walls using the AFM topography and recognition (TREC) technique and the dynamic force spectroscopy with a CBM3a functionalized AFM tip (Figure 4). The AFM tip was first coated with a magnetic material followed by a layer of gold. The gold surface of the tip was then modified with thiol−$PEG_{2000}$−NTA−Ni cross-linker and CBM3a molecules, using a procedure similar to the GNP modification (see details described in Supporting Information, SI-IV). Figure 4a shows a schematic of a modified AFM tip and the binding of CBM3a molecule on planar crystalline cellulose chains. Unlike the GNP functionalization, a longer and more flexible $PEG_{2000}$ was used here as the major portion of cross-linker to minimize


dx.doi.org/10.1021/jp304686q | J. Phys. Chem. B 2012, 116, 9949−9956

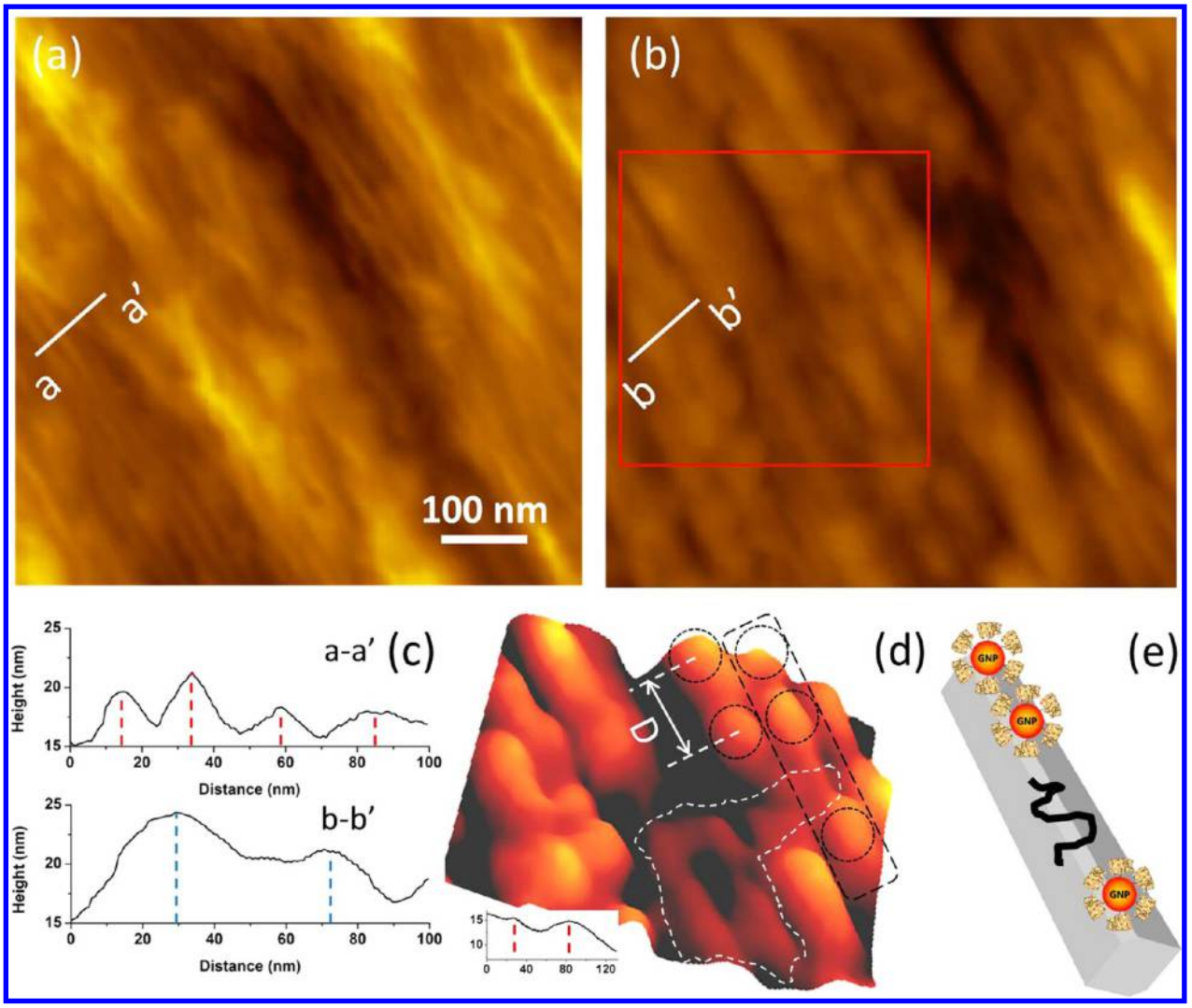


**Figure 3.** Morphology of the cell wall surface before and after GNP−CBM3a's binding to the cellulose: (a) before binding; (b) after binding; (c) cross-section profile of the white lines a−a′ in part a and b−b′ in part b; (d) highlighted 3D image of representative alignment of the complexes marked in the red square (inset: cross-section profile of two adjacent GNP−CBM3a complexes labeled by double-headed arrow from the center). The center of the cellulose microfibrils and bound GNP−CBM3a complexes are marked by dashed red and dashed blue lines, respectively in part c. GNP−CBM3a complexes bound on the cellulose surface were partially highlighted by dashed, black circles. The dashed white lines in part d highlight the center of the two adjacent complexes and the distance in-between marked by letter "*D*" is about 50 nm, indicating the space between the edges of two bound particles is 20−30 nm. The cellulose microfibrils uncovered are marked by the dashed white circle. The single alignment of GNP−CBM3a complexes on the hydrophobic (110) surface of a single cellulose microfibril is marked by a dashed black rectangle and highlighted as the schematics in part e.

the misorientation and steric hindrance.[38] The gold−NTA−Ni−$(His)_6$-tagged protein is a widely used chelating complex due to its specificity, affinity and remarkable stability in the environment of high salt, wide pH range and various solvents.[35]

It has been established that at least three aromatic residues on a CBM surface are required for cellulose-CBM binding activity.[39] The conserved flat surface on the bottom of the CBM3a is proposed to interact hydrophobically and selectively with the (110) face of crystalline cellulose, involving five amino acid residues which form a planar strip (the residues are not shown in the figure).[15] As shown in Figure 4b-e, the cellulose fibrils are clearly seen in the topography image (left, Figure 4b) and the corresponding recognition signals are generated at the same locations on the recognition image (right, Figure 4c).[40] The dashed, red lines in both Figure 4d and Figure 4e indicate the obvious correspondence between the recognition signals and the morphology of the crystalline cellulose as observed in topographic images (Figure 4b). Also, the dark areas in the recognition image correspond very well to the areas where the cellulose fibrils are located in the topographic images, indicating that the CBM3a molecules bound to the crystalline cellulose surface successfully during the scanning. We noticed that not the whole cellulose area was completely recognized by the modified AFM probe, which is expected given the impurity of the cellulose surface and the inevitable misorientation of the binding sites on CBM3a during scanning. As a result, not all the single binding sites were distinguishable on this scale. On average, 70−80% of the binding area can be recognized based on the experimental observations based on the analysis of 10 recognition images of crystalline cellulose (each in size of 300 nm × 300 nm).

To reveal the single binding sites, we focused on a smoother segment on the topographic and recognition profiles for a closer look at the correspondence of the recognition events. As


dx.doi.org/10.1021/jp304686q | *J. Phys. Chem. B* 2012, 116, 9949−9956

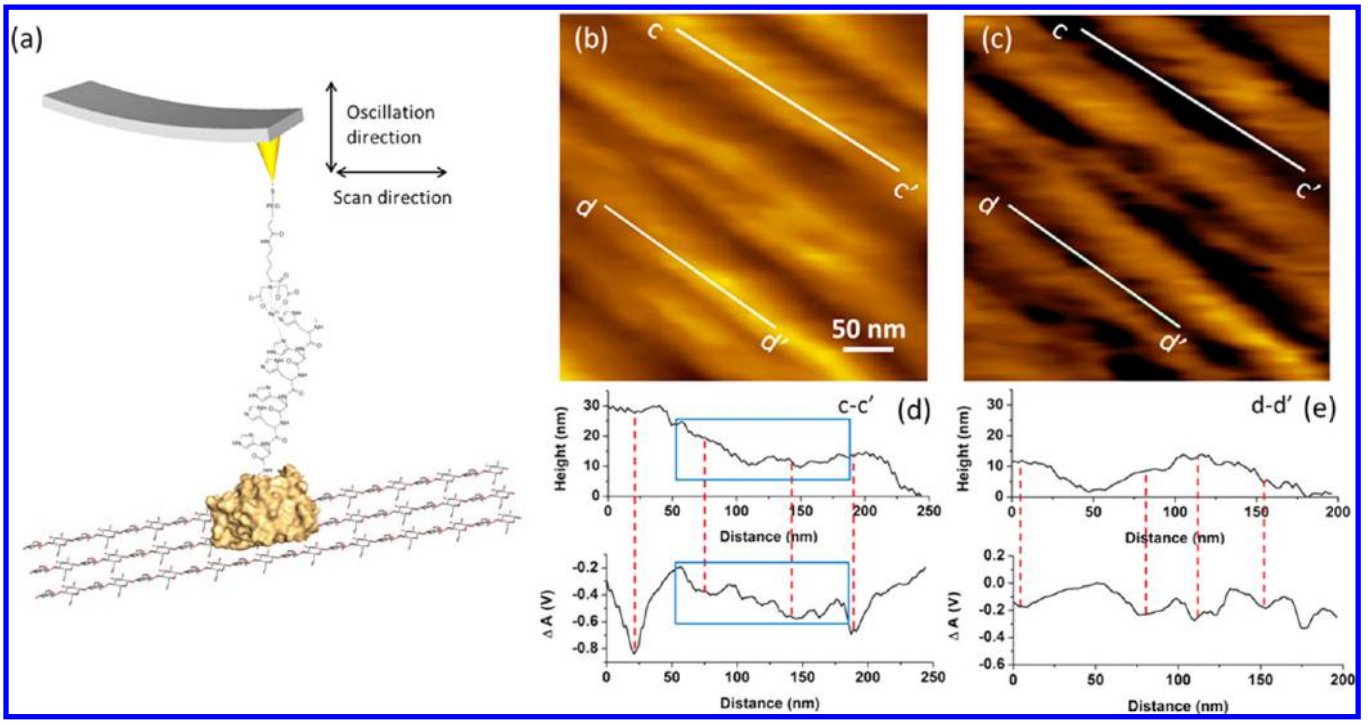


**Figure 4.** Schematics of a modified AFM tip and AFM Topographic and Recognition images of the CBM3a-cellulose interaction: (a) schematics of a modified AFM tip with CBM3a binding to the cellulose surface; (b) topographic image; (c) recognition image, where two representative cellulose fibrils with recognition signals are highlighted in white lines and the corresponding cross-section profiles are shown in parts d (following line c−c′) and e (following line d−d′), respectively. The upper profiles are generated from topographic image and the lower ones are generated from recognition image in both parts d and e. $\Delta A$: Amplitude difference in the recognition signal.[40] The dashed, red lines in both parts d and e indicate the correspondence of the recognition signals to the morphology of the crystalline cellulose shown in part b.

shown in Figure 5, most binding sites were clearly observable and the binding site intervals were measurable from the

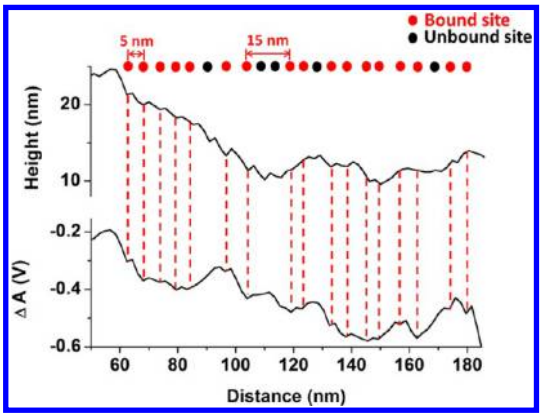


**Figure 5.** Zoom-in binding site intervals measured from the recognition profile of c−c′ cross-section in Figure 4d. The red dot indicates the recognition event (bound site); the black dot indicates the missing recognition events (unbound site). The dashed red lines are shown to guide the correspondence of the recognition events to the signal changes in profiles.

recognition profile of c−c′ cross-section as highlighted in the blue square in Figure 4d. In Figure 5, the red and black dots in diameter of about 3 nm (close to the size of single binding site) above each line indicate the recognition event (bound sites) and missed recognition events (unbound sites), respectively. The signal changes in the recognition profile correspond to the dips and bumps in the topographic profile randomly, which means that the recognition signals were generated due to the specific binding sites instead of the surface roughness. Additionally, the minimum distance between the centers of two bound sites (red dots) is measured to be 5−8 nm, deducing a separation distance of 2−5 nm, which is in the range of the separation distance guided by quantum dots as discussed above. Some larger distances of 10−15 nm were also observed and are suggestive of separation by 1 or 2 unbound events. We speculate that these missing binding events are caused by short binding time under relatively fast scanning speed and impurity of the natural cell wall cellulose. On the basis of the analysis of 50 cross-section curves from the recognition area, 41 curves (over 80%) show similar binding distributions. To further prove the above results, a control experiment using a bare AFM tip was carried out, indicating the absence of specific interactions and binding sites between the cell wall cellulose and bare tip (Supporting Information, SI-V).

On the basis of the above findings, we set to quantify the binding affinity by measuring the unbinding forces between the single CBM3a molecule and a small area of crystalline cellulose on the poplar sample surface. To ensure the statistic data was reliable, 1000 force distance curves were collected under the loading rate of 67.2 nN/s to construct a force histogram. The Gaussian-fitted peak value represented the most probable unbinding force (Figure 6). Using the CBM3a-functionalized tip, two peaks (blue in Figure 6) were generated, showing simultaneously the specific (right, lower and wider peak) and nonspecific (left, higher and narrower peak) interactions between the CBM3a and sample surface. Using the typical force curves (type II curves in Figure 6 which comprises 48% of the total curves), the unbinding force between the single CBM3a molecule and the crystalline cellulose was determined


dx.doi.org/10.1021/jp304686q | J. Phys. Chem. B 2012, 116, 9949−9956

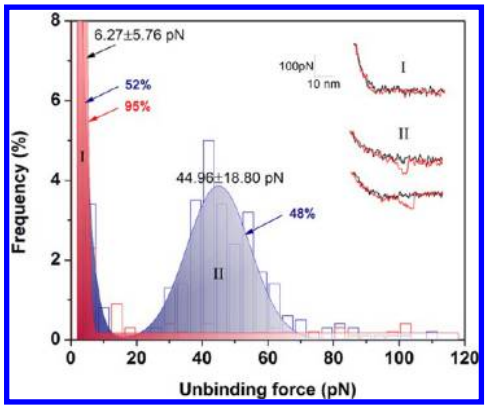


**Figure 6.** Histogram and representative force–distance curves of the CBM3a-cellulose binding interactions with specific and nonspecific interaction. The blue area under Gaussian fitting curve indicates both the specific (labeled as II, the same for representative curves) and nonspecific (labeled as I, the same for representative curve) interactions between the cell wall cellulose and CBM3a-functionalized AFM tip. The red area shows the nonspecific interactions between the cellulose and the bare AFM tip in the control experiment. A total of 1000 curves were collected for each experiment to construct the histogram for the fitting. Key: trace curves, black; retrace curves, red. The unbinding force between the CBM3a and crystalline cellulose is determined to be 44.96 ± 18.8 pN from Gaussian fitting under the loading rate of 67.2 nN/s.

to be 44.96 ± 18.80 pN under the loading rate of 67.2 nN/s by Gaussian fitting. The remaining 52% of the curves (type II curves in Figure 6) showed no evident binding as only 6.27 ± 5.76 pN force was determined in the histogram. Using a bare AFM tip, 95% of the obtained force curves are the type I curves and by Gaussian fitting (red in Figure 6) it gives the same result as the no binding peak using the CBM3a-functionalized tip.

We noticed that the unbinding force of CBM3a and crystalline cellulose is much smaller than that needed to break a covalent bond (larger than 1 nN at the loading rate of 10 nN/s),[41] or that between antibody and antigen,[42] thereby indicating a weaker interaction between CBM3a and cellulose. According to previous works, the protein-carbohydrate affinity brought about by the conserved aromatic residues in the planar strip and two adjacent anchoring residues at the bottom surface of CBM3a mainly relies on hydrophobic van der Waals contacts, with partial contribution by the polarization interactions between the polar side-chains of aromatic residues and the pyranose rings located on the (110) face of crystalline cellulose.[20,43] Replacement of the above binding residues with alanine has shown a great increase in dissociation constant of the binding module, indicating a much weaker binding affinity due to the absence of the aromatic, hydrophobic interactions.[44] We speculate that the nonspecific peak measured in Figure 6 is mainly attributed to the misorientation of the CBM3a molecule on the cellulose surface or the feeble interactions between CBM3a and noncrystalline cellulose component on the sample surface.

## CONCLUSIONS

In this work, we used the CBM3a-modified gold nanoparticles to determine the behavior of the CBM3a, a crystalline cellulose-binding module, on natural cellulose surface. We observed that the GNP–CBM3a complexes bound to the cellulose surface and closely aligned with the cellulose extension. The binding behavior was proved to be real after comparing the topographic and recognition images of the same crystalline cellulose exposed area as well as the force measurement done by dynamic force microscopy. Quantitatively, the unbinding force between the CBM3a and crystalline cellulose was determined as 44.96 ± 18.80 pN under the loading rate of 67.2 nN/s. To further determine the CBM-cellulose interaction, additional unbinding forces under different loading rates need to be tested, and other types of type A CBMs should be selected to quantitatively measure their differences in binding affinities. Dissection of the binding mechanism of cellulose-specific CBMs at the single-molecule level may lead to better understanding of biomass–enzyme interactions, thus facilitating the design of high-efficiency cellulolytic enzymes.

## ASSOCIATED CONTENT

### Supporting Information

Preparation of recombinant CBM3a (SI-I), synthesis of DTSP-ANTA cross-linker (SI-II), control experiments of AFM imaging (SI-III and SI-V), and AFM tip functionalization (SI-IV). This material is available free of charge via the Internet at http://pubs.acs.org.

## AUTHOR INFORMATION

### Corresponding Author

*E-mail: bxu@engr.uga.edu.

### Notes

The authors declare no competing financial interest.

## ACKNOWLEDGMENTS

We gratefully thank National Science Foundation (ECCS 0823849, CBET 1139057) for financial support of this research. We also sincerely thank the Electron Microscopy (EM) Laboratory of the Department of Plant Biology, University of Georgia, in helping in using the microtome facility.

## REFERENCES

(1) Somerville, C.; Bauer, S.; Brininstool, G.; Facette, M.; Hamann, T.; Milne, J.; Osborne, E.; Paredez, A.; Persson, S.; Raab, T.; et al. *Science* **2004**, *306*, 2206–2211.
(2) Himmel, M. E.; Ding, S. Y.; Johnson, D. K.; Adney, W. S.; Nimlos, M. R.; Brady, J. W.; Foust, T. D. *Science* **2007**, *315*, 804–807.
(3) Cosgrove, D. J. *Nat. Rev. Mol. Cell Biol.* **2005**, *6*, 850–861.
(4) Stocker, M. *Angew. Chem., Int. Ed.* **2008**, *47*, 9200–9211.
(5) Grabber, J. H. *Crop Sci.* **2005**, *45*, 820–831.
(6) Girio, F. M.; Fonseca, C.; Carvalheiro, F.; Duarte, L. C.; Marques, S.; Bogel-Lukasik, R. *Bioresour. Technol.* **2010**, *101*, 4775–4800.
(7) Zhu, J. Y.; Pan, X. J. *Bioresour. Technol.* **2010**, *101*, 4992–5002.
(8) Jordan, D. B.; Bowman, M. J.; Braker, J. D.; Dien, B. S.; Hector, R. E.; Lee, C. C.; Mertens, J. A.; Wagschal, K. *Biochem. J.* **2012**, *442*, 241–252.
(9) Zhang, Y. H. P.; Lynd, L. R. *Biotechnol. Bioeng.* **2004**, *88*, 797–824.
(10) Gilbert, H. J. *Plant Physiol.* **2010**, *153*, 444–455.
(11) Smith, L. G. *Nat. Rev. Mol. Cell Bio.* **2001**, *2*, 33–39.
(12) Wang, W.; Yuan, T.; Wang, K.; Cui, B.; Dai, Y. *Bioresour. Technol.* **2012**, *107*, 282–286.
(13) Boraston, A. B.; Bolam, D. N.; Gilbert, H. J.; Davies, G. J. *Biochem. J.* **2004**, *382*, 769–781.
(14) Cantarel, B. L.; Coutinho, P. M.; Rancurel, C.; Bernard, T.; Lombard, V.; Henrissat, B. *Nucleic Acids Res.* **2009**, *37*, D233–D238.
(15) Tormo, J.; Lamed, R.; Chirino, A. J.; Morag, E.; Bayer, E. A.; Shoham, Y.; Steitz, T. A. *Embo J.* **1996**, *15*, 5739–5751.
(16) Blake, A. W.; McCartney, L.; Flint, J. E.; Bolam, D. N.; Boraston, A. B.; Gilbert, H. J.; Knox, J. P. *J. Biol. Chem.* **2006**, *281*, 29321–29329.

(17) Nishiyama, Y. L.; Langan, P.; Chanzy, H. *J. Am. Chem. Soc.* **2002**, *124*, 9074−9082.
(18) Kawakubo, T.; Karita, S.; Araki, Y.; Watanabe, S.; Oyadomari, M.; Takada, R.; Tanaka, F.; Abe, K.; Watanabe, T.; Honda, Y. *Biotechnol. Bioeng.* **2010**, *105*, 499−508.
(19) Mccann, M. C.; Wells, B.; Roberts, K. *J. Cell Sci.* **1990**, *96*, 323−334.
(20) Lehtio, J.; Sugiyama, J.; Gustavsson, M.; Fransson, L.; Linder, M.; Teeri, T. T. *Proc. Natl. Acad. Sci. U.S.A.* **2003**, *100*, 484−489.
(21) Xu, Q.; Tucker, M. P.; Arenkiel, P.; Ai, X.; Rumbles, G.; Sugiyama, J.; Himmel, M. E.; Ding, S. Y. *Cellulose* **2009**, *16*, 19−26.
(22) Filonova, L.; Kallas, A. M.; Greffe, L.; Johansson, G.; Teeri, T. T.; Daniel, G. *Biomacromolecules* **2007**, *8*, 91−97.
(23) Machado, J.; Araujo, A.; Pinto, R.; Gama, F. M. *Cellulose* **2009**, *16*, 817−824.
(24) Tetard, L.; Passian, A.; Thundat, T. *Nat. Nanotechnol.* **2010**, *5*, 105−109.
(25) Muller, D. J.; Dufrene, Y. F. *Nat. Nanotechnol.* **2008**, *3*, 261−269.
(26) Ding, S. Y.; Himmel, M. E. *J. Agr. Food Chem.* **2006**, *54*, 597−606.
(27) Tetard, L.; Passian, A.; Farahi, R.; Kalluri, U.; Davison, B.; Thundat, T. *Ultramicroscopy* **2010**, *110*, 701−707.
(28) Liu, H.; Fu, S.; Zhu, J.; Li, H.; Zhan, H. *Enzyme Microb. Technol.* **2009**, *45*, 274−281.
(29) Igarashi, K.; Koivula, A.; Wada, M.; Kimura, S.; Penttila, M.; Samejima, M. *J. Biol. Chem.* **2009**, *284*, 36186−36190.
(30) Liu, Y. S.; Baker, J. O.; Zeng, Y.; Himmel, M. E.; Haas, T.; Ding, S. Y. *J. Biol. Chem.* **2011**, *286*, 11195−11201.
(31) Zhong, L.; Matthews, J. F.; Crowley, M. F.; Rignall, T.; Talon, C.; Cleary, J. M.; Walker, R. C.; Chukkapalli, G.; McCabe, C.; Nimlos, M. R.; et al. *Cellulose* **2008**, *15*, 261−273.
(32) Mulakala, C.; Reilly, P. J. *Proteins* **2005**, *60*, 598−605.
(33) Hinterdorfer, P.; Dufrêne, Y. F. *Nat. Methods* **2006**, *3*, 347−355.
(34) Ebner, A.; Kienberger, F.; Kada, G.; Stroh, C. M.; Geretschlager, M.; Kamruzzahan, A. S. M.; Wildling, L.; Johnson, W. T.; Ashcroft, B.; Nelson, J.; et al. *Chemphyschem* **2005**, *6*, 897−900.
(35) Hainfeld, J. F.; Liu, W.; Halsey, C. M.; Freimuth, P.; Powell, R. D. *J. Struct. Biol.* **1999**, *127*, 185−198.
(36) Jain, P. K.; Huang, X.; El-Sayed, I. H.; El-Sayad, M. A. *Plasmonics* **2007**, *2*, 107−118.
(37) Kuhle, A.; Sorensen, A. H.; Zandbergen, J. B.; Bohr, J. *Appl. Phys. A: Mater.Sci. Process.* **1998**, *66*, S329−S332.
(38) Chen, G. J.; Zhou, J. F.; Park, B.; Xu, B. Q. *Appl. Phys. Lett.* **2009**, *95*, 043103.
(39) Shimon, L. J. W.; Pages, S.; Belaich, A.; Belaich, J. P.; Bayer, E. A.; Lamed, R.; Shoham, Y.; Frolow, F. *Acta Crystallogr., Sect. D: Biol. Crystallogr.* **2000**, *56*, 1560−1568.
(40) Stroh, C.; Wang, H.; Bash, R.; Ashcroft, B.; Nelson, J.; Gruber, H.; Lohr, D.; Lindsay, S. M.; Hinterdorfer, P. *Proc. Natl. Acad. Sci. U.S.A.* **2004**, *101*, 12503−12507.
(41) Grandbois, M.; Beyer, M.; Rief, M.; Clausen-Schaumann, H.; Gaub, H. E. *Science* **1999**, *283*, 1727−1730.
(42) Zlatanova, J.; Lindsay, S. M.; Leuba, S. H. *Prog. Biophys. Mol. Biol.* **2000**, *74*, 37−61.
(43) Toone, E. J. *Curr. Opin. Struc. Biol.* **1994**, *4*, 719−728.
(44) Murashima, K.; Kosugi, A.; Doi, R. H. *J. Bacteriol.* **2005**, *187*, 7146−7149.